Available online at www.sciencedirect.com
SCIENCE DIRECT
Polymer 47 (2006) 489–497
polymer
www.elsevier.com/locate/polymer

# Application of an interpenetrating network model to the necking in the microcrystalline region in four annealed isotactic polypropylene films subjected to uniaxial stretching at room temperature ☆

Yihu Song [a,*], Norio Nemoto [b]

[a] Institute of Polymer composite, Department of Polymer Science and Engineering, Zhejiang University, Hangzhou 310027, China
[b] Department of Molecular and Material Sciences, IGSES, Kyushu University, Hakozaki, Fukuoka 812-8581, Japan

Received 4 November 2004; received in revised form 25 March 2005; accepted 3 May 2005
Available online 21 November 2005

**Abstract**

The microscopic infrared dichroism, mesoscale deformation and macroscopic stress measurements are made on the microcrystalline region in four annealed isotactic polypropylene (iPP) thin films subjected to uniaxial stretching at room temperature. Results reveal that volume dilatation might occur during stretching and the necking causes the anisotropic shrinkage in the thickness and the width directions. The average orientation function $f_{av}$ and the true stress as a function of local draw ratio in the samples showing volume dilatation can be respectively overlapped onto those of the sample undergoing constant volume deformation. The pseudo-affine deformation is applicable for molecular orientation at $f_{av} < 0.50$ and the true stress–strain relationship on the mesoscale can be well described in the same region by the interpenetrating network model previously proposed for necking in the quenched iPP film. This model becomes invalid for deformations above $f_{av} = 0.50$ due to that plastic deformations in the crystalline phase, depending on the annealing time, start to play a major role.


*Keywords:* Isotactic polypropylene film; Annealing; Deformation

## 1. Introduction

Semicrystalline polymers being composed of crystalline lamellae and entangled amorphous chains show a complicated behavior under tensile strain. They exhibit large plasticity when being deformed above the glass transition temperature $T_g$ of the amorphous phase [1]. The structure–mechanical property relations have been investigated on levels of crystal-lattice and lamella as well as large-scale superstructures such as spherulites [2]. However, the inhomogeneous structural nature on both microscopic and macroscopic scales makes it quite difficult to understand molecular orientation mechanisms underlying the tensile behavior on the basis of direct observation of the localized plastic deformations. While microstructural deformations in spherulites and microcrystalline region are well documented [3], their contributions to macroscopic behaviors are still ambiguous [4]. Therefore, it is difficult to establish a straightforward relationship between the microstructural deformations and the applied macroscopic stress. On the other hand, Strobl and coworkers have performed extensive investigations on the deformation mechanisms utilizing true stress–strain measurements at constant strain rates [5] and argued that stretching of the amorphous network dominates the deformation at strains beyond the yield point where a critical stress is attained for destructing crystallites.

Using an equipment for simultaneous kinetic measurements of microscopic infrared (MicIR) dichroism from a predetermined mesoscale sampling area and of macroscopic stress of a polymer film subjected to uniaxial stretching at a constant elongation rate [6], we studied the molecular orientation of a quenched isotactic polypropylene (iPP) film during necking at room temperature [7]. The deformation is truly inhomogeneous on a macroscopic scale. However, drastic deformation and molecular orientation mainly occur in the neck shoulder [8]. We disclosed a pseudo-affine deformation up to a local draw ratio $\lambda_L \sim 4.5$ determined on a mesoscale of

☆ Part VII of deformation mechanisms of polymer thin films by simultaneous kinetic measurements f microscopic infrared dichroism and macroscopic stress.

* Corresponding author. Tel.: +86 571 879 53075.
*E-mail address:* s_yh0411@zju.edu.cn (Y. Song).

0032-3861/$ - see front matter © 2005 Elsevier Ltd. All rights reserved.
doi:10.1016/j.polymer.2005.05.159

200 μm, i.e. the film shrinks anisotropically in the width and the thickness directions whereas the molecular orientation function in the amorphous phase, $f_{am}$, as a function of $\lambda_L$ could be described by the affine deformation model. Since the orientation function of the crystalline phase, $f_c$, has been found to be in proportion to $f_{am}$ in the same $\lambda_L$ region [8], the average orientation function of molecules in both phases, $f_{av}$, as a function of $\lambda_L$ can also be described by the affine model. By measuring the molecular orientation along the draw axis of a quenched film stretched to different macroscopic strains, we showed that $f_{am} \approx 0.45$ is the upper limit of the pseudo-affine deformation occurring in the narrow neck shoulder region [9]. This $f_{am}$ value agrees with the theoretical prediction on the highest value attainable for the ideal rubber network and partly explains why the neck shoulder appears to propagate smoothly.

We proposed an interpenetrating network model for interpreting the true stress–strain relationship of a mesoscale area suffering from necking in the quenched iPP film [9]. In this model, a small portion of crystallites adhered through intercrystalline links [10] forms a rigid crystal (C) network that penetrates through a soft crystallite enhanced amorphous matrix (CEAM) network. The deformation of the C network during the necking is described using Takayanagi-Nitta tie molecule model [11], while that of the CEAM network should obey the pseudo-affine deformation model as far as the test temperature is above the glass transition temperature. For the quenched iPP film, this model is able to account for inhomogeneous deformation accompanied with the localized necking at draw temperatures below 400 K where crystallinity does not change markedly [12]. This model with slight alteration is also valid for uniaxial deformation of films of poly(ether-*block*-amide) multiblock copolymers [13] and also films of a metallocene polypropylene, and an ethylene-butylene rubber and their 80 wt/20 wt blend at room temperature [14].

It is well known that annealing of iPP film results in various sizes of spherulites with the α-form, which significantly influences the mechanical properties of the final products. Large spherulites often promote brittleness owing to the concentration of structural defects at their boundaries [15]. In investigation of the $f_c$–$f_{am}$ relation for the microcrystalline region of annealed iPP films, we noticed that deformation behaviors of a giant spherulite with a diameter of several hundreds of micron are quite different from that of the microcrystalline region, i.e., a giant spherulite could resist the elongational stress by local lamellar rearrangement and shows plastic deformation upon stress concentration [16]. Cracking usually initiates at the spherulite boundary and propagates toward the drawing axis over a pretty long distance. The interpenetrating network model could not describe the inhomogeneous deformation of a film containing both microcrystalline region and spherulites, but would be useful for discussing the true stress–strain relationship during the localized deformation of the microcrystalline region itself among spherulites. Since the cooperativity of the crystalline and the amorphous phases or relative contributions of the two networks in the proposed model might be influenced by fine morphologies formed at various annealing conditions, we in this study further examine the applicability of the interpenetrating network model to the plastic deformation in the microcrystalline region of four iPP films annealed at different conditions. The average size of spherulites in iPP films increases with increasing time of isothermal annealing. However, the influences of annealing condition on the structure in the microcrystalline region and also on the room temperature deformation are not yet clear. We in this study attempt to reveal such aspect executing the MicIR dichroism, mesoscale deformation and macroscopic stress measurements and analyzing the data in the framework of the interpenetrating network model.

## 2. Experimental section

### 2.1. Materials and sample preparation

iPP pellets with $M_w = 3.7 \times 10^5$ g mol$^{-1}$ were compressed at 210 °C for 5 min to form a film with an average thickness of ca. 30 μm, which was then transferred to an oven and annealed at four different conditions. Fig. 1(a) shows the typical morphologies of the films containing giant spherulites with the α-type of crystal structure. When the film was annealed at 145 °C, the average size of spherulite increased with time and a spherulitic embryo without Maltese cross was observed after annealing of 4 h. The size of spherulite after annealing at 140 °C for 2 h was smaller than at the other three conditions.

### 2.2. Apparatus and method

The setup detail of the equipment, the kinetic measurement of MicIR dichroism and the data analysis procedure are described in earlier papers [7,8].

The prepared films were observed under polarized optical microscope and a region satisfying the specially designed experiment was selected and carefully cut into a rectangle sample with an initial width $W_0 = 3$ mm. In the desired working section of the sample, the distance between spherulites was at least 3 mm along the longitudinal direction. The samples were fastened between the two clamps and were stretched at a constant elongation rate of 0.05 min$^{-1}$ with simultaneous movement of the clamps to the two opposite directions. The initial length $L_0$ between the two clamps was adjusted as 2 mm. After stretching the samples, the working section was observed under a polarized microscope in order to ensure that it did not contain any spherulite with distinguishable Maltese cross. Fig. 1(b) and (c) shows the micrographs of the microcrystalline region at macroscopic draw ratios 1 and 8, respectively.

The measurements were performed at 30.0 ± 0.1 °C. The viewing field for sampling of the MicIR dichroism signal was $200 \times 200$ μm$^2$. Before stretching the films, a sampling area was predetermined as that exactly located in the film center where several hard objects in a size of 10–20 μm could be distinguished under the microscope. These objects differ from spherulites and may have been formed during crystallization. One of the objects was pursued and adjusted to the viewing

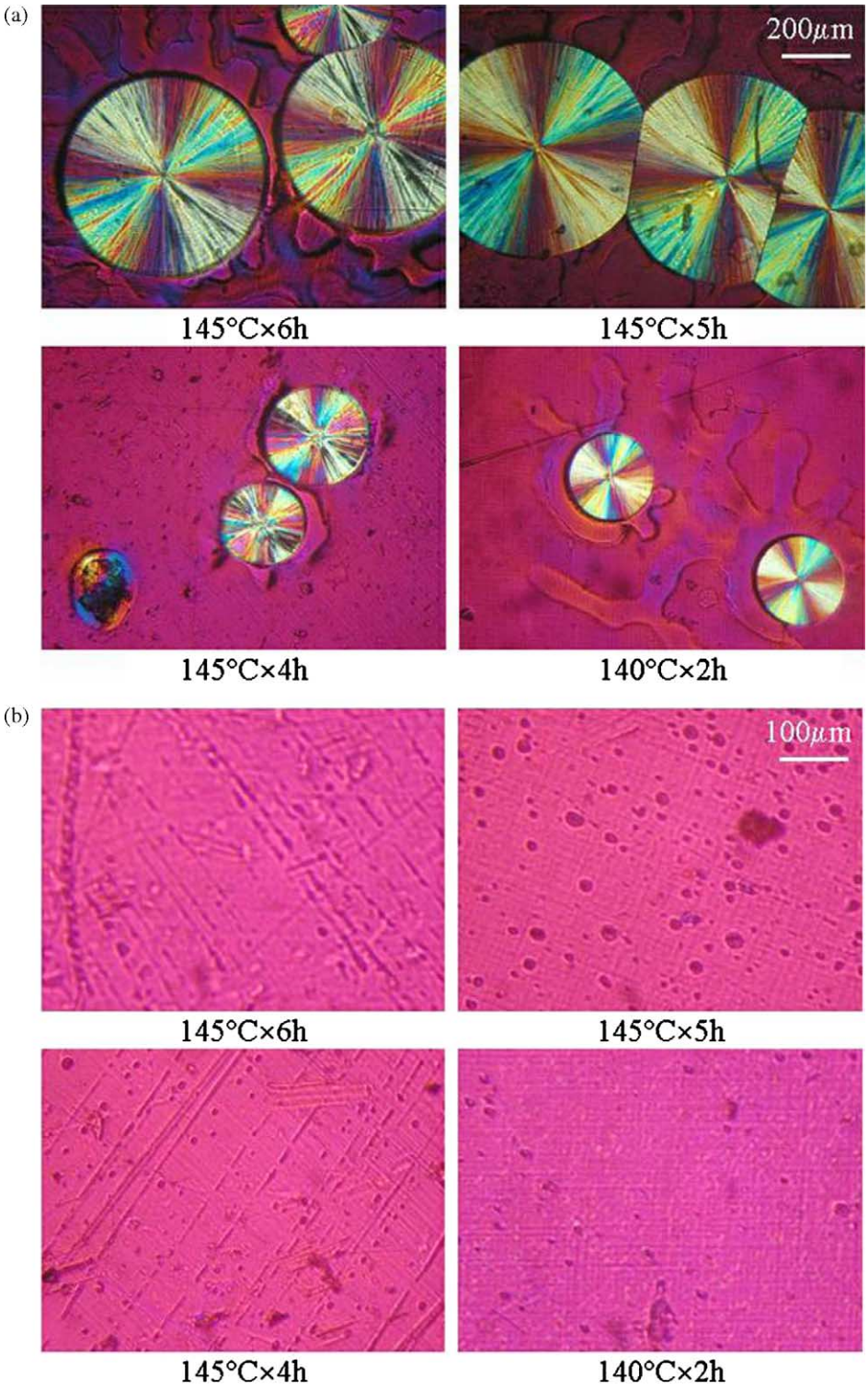


Fig. 1. Polarized optical micrographs of the films annealed at 145 °C for 6, 5 and 4 h and at 140 °C for 2 h (a), and of the microcrystalline region at two macroscopic draw ratios $\lambda_{Mac}=1$ (b) and $\lambda_{Mac}=8$ (c). The heavy arrow in part (c) shows the draw direction. Before deformation, the microcrystalline region in the annealed films contains considerably abundant crystal-like domains with irregular shapes and with a size from several microns to several decades of micron. At $\lambda_{Mac}=8$ (c), most of these domains are highly elongated with their long axes parallel to or near parallel to the draw axis. Several domains without obvious deformation can also be distinguished. The sample 140 °C×2 h shows a mechanical breakup of an original existed crystal aggregate, the residues being separated along the draw direction.

field under the microscope at a given time interval of 3 min moving the $x$–$y$–$z$ stage supporting the sample cell. A digital camera (Camedia C4040Z00M, Olympus Optical Co. Ltd.) connected with the ocular of the IR microscope was used to record micrographs of the sampling area just after the adjustment. The method of photogrammetry was employed for in situ determination of the local strains within the sampling area to individual samples [8]. Distances between the objects in

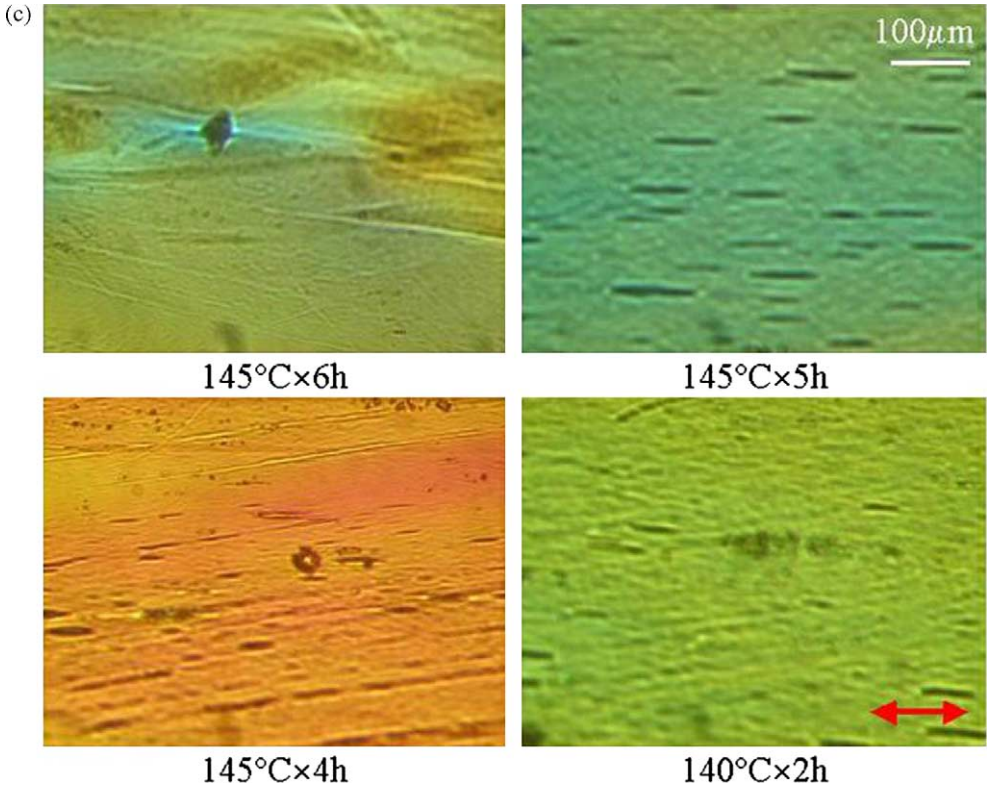


Fig. 1 (*continued*)

the sampling area were read from the micrographs in order to evaluate $\lambda_L$ in the stretching direction and the relative local width $\lambda_w$ in the perpendicular direction. The relative local thickness $\lambda_d$ was monitored using the structural absorbance ratio $A_0(t)/A_0(0)$ of the thickness-sensitive band at 973 $cm^{-1}$ belonging to the $CH_3$ rocking and the axial and equatorial C–C stretching modes in both the amorphous and the crystalline phases [17]. The true stress $\sigma$ to the pursued sampling area was calculated from $\sigma = \sigma_n/(\lambda_w\lambda_d)$. Here, $A_0(t)$ and $A_0(0)$ are the structural absorbance at stretching time $t$ and zero, respectively, and $\sigma_n$ is the nominal stress read from the elongation device. Only data from the samples with a mark distinguishable up to the end of stretching were analyzed.

The orientation function, $f_{av}$, in relation to the average chain orientation of both the amorphous and the crystalline phases in the close vicinity of the sampling area was derived from the π-band at 973 $cm^{-1}$ [18]. The $f_c$ was determined from the π-band at 998 $cm^{-1}$ involving the $CH_3$ rocking, the C–$CH_3$ stretching, the CH bending and the $CH_2$ twisting modes in the crystalline phase.

## 3. Results and discussion

### *3.1. Nominal stress and molecular orientation*

Fig. 2(a) shows the time profiles of nominal stress $\sigma_n$. The films yield at $t = 3.5$–$4.9$ min. The nominal yielding stress varies with annealing condition. The two samples 145 °C × 5 h and 140 °C × 2 h show the lowest and the highest nominal yielding stress, respectively. A small sharp stress peak is observed at $t = 13.4$–$14.6$ min during the strain softening for the films annealed at 145 °C, which is different from the strain softening of the quenched film and also of the film annealed at 140 °C.

As shown in our previous studies [7–9,16], the time dependence of molecular orientation function from a predetermined sampling area in iPP film is not monotonous but is closely related to the location of this small area with respect to the neck developed during stretching. Molecules are less or slightly deformed when the sampling area is located outside the neck or in the highly necked-down region namely the neck entity. A dramatic molecular deformation is undoubtedly involved in the necking propagation through the sampling area, accompanied by a rapid transformation of molecules from the random to the highly oriented alignment. Fig. 2(b) shows the time profiles of average molecular orientation function $f_{av}$ for the four annealed films. Though the necking was initiated in a position close to the original film center, the shape of neck shoulder and the rate of necking propagation are different in these four samples. The rapid increment in $f_{av}$ always occurs during the necking propagation through the sampling area [8], whereas, the different slopes in Fig. 2(b) are ascribed to the different shape evolution of the neck shoulder. In samples 145 °C × 6 h and 145 °C × 5 h, the necking propagation through the sampling area causes a smooth increase in $f_{av}$ against $t$ with almost the same slope. On the other hand, the

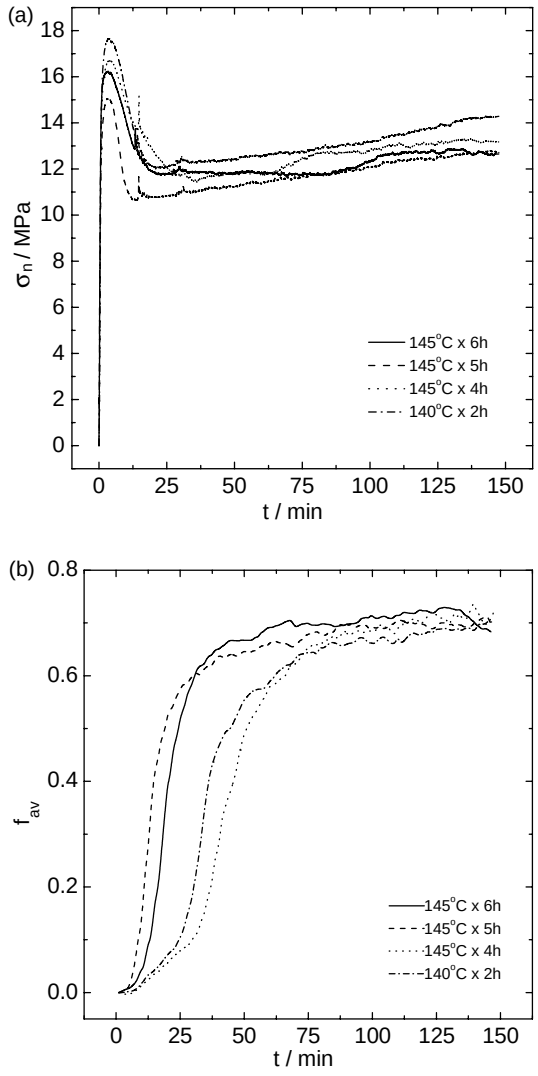


Fig. 2. Nominal stress $\sigma_n$ (a), and average orientation function $f_{av}$ (b) as a function of the stretching time $t$.

slope of $f_{av}$ against $t$ shows a discontinuous change at $f_{av}=0.1$, or $t=25$ and 30 min, respectively, in samples 145 °C×4 h and 140 °C×2 h. The neck shoulder in the later two samples might not be stable but its geometry varies along with propagation. The molecular orientation develops considerably slowly at $f_{av}>0.5$ where the necking has passed through the sampling area, suggesting that deformation in the neck entity proceeds via another fashion differing from that in the neck shoulder.

### 3.2. Relationship between $f_c$ and $f_{av}$

The relationship between $f_c$ and $f_{av}$ is presented in Fig. 3 in which $f_c$ of each sample is vertically shifted by a shift factor $b_s$. A linear portion in the $f_c$–$f_{av}$ relationship could be distinguished at $f_{av}\leq 0.5$. For two samples annealed at 145 °C×5 h (–, 3), the necking was initiated at different positions with respect to the predetermined sampling area, nevertheless their $f_c$–$f_{av}$ relationships were identical to each other. The slope $K'$ of the linear portion is determined as 1.2, 1.4, 1.3 and 1.4 for the samples 145 °C×6 h, 145 °C×5 h, 145 °C×4 h, and 140 °C×2 h,

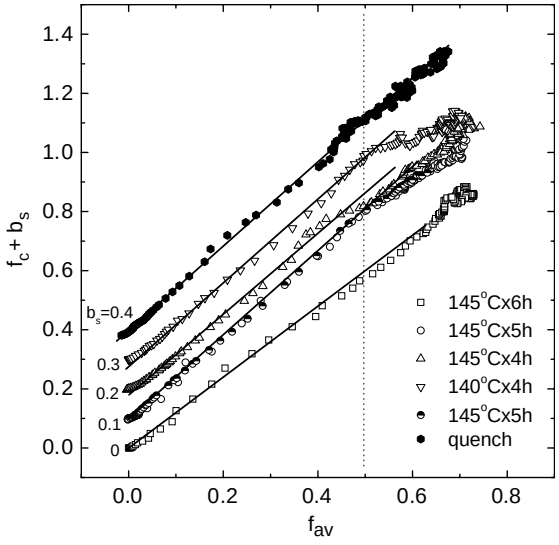


Fig. 3. Relationship between the crystalline orientation function $f_c$ and the average orientation function $f_{av}$.

respectively, which is comparable to the value of $K'\approx 1.4$ in the quenched sample. The slight differences may be related to the degree of average local crystallinity in the sampling area. The result in Fig. 3 suggests that a linear relationship between $f_c$–$f_{am}$ should also hold in the annealed iPP samples whenever crystallinity does not change significantly, especially in the deformation before the necking passes through the sampling area.

### 3.3. Local deformation

Fig. 4 shows the local extension ratios $\lambda_L$ and $\lambda_W$ determined from micrographs of the sampling area, as well as $\lambda_d$ estimated from the relative structural absorbance of the band at 973 $cm^{-1}$. The films shrink equally in the thickness and the width directions at the earlier stage of stretching, whereas, $\lambda_d$ eventually becomes smaller than $\lambda_w$. Essentially the same deformational anisotropy has been found for the quenched film and appears as a general characteristic of the necking in iPP microcrystalline region [8,9]. Comparison of Figs. 2(b) with 4 reveals that the dramatic molecular orientation and longitudinal extension develop in a harmonious fashion, both being due to the transformation of the sampling area from the isotropic state to the highly deformed anisotropic one. After the neck passes away, the sampling area slowly deforms, which gives rise to the slow increase in local extension ratios.

By assuming a value of Poisson's ratio $\nu$ being identical in the whole deformation process, we calculated the local draw ratio from the measured $\lambda_W$ and $\lambda_d$ according to $\lambda_L=(\lambda_w\lambda_d)^{-1/2\nu}$, as shown by the solid curves in Fig. 4. We found that $\nu=0.40$, 0.47, 0.50 and 0.41 as values for the best fitting describes the local geometrical evolution of the samples 145 °C×6 h, 145 °C×5 h, 145 °C×4 h, and 140 °C×2 h, respectively. This result implies that the microcrystalline region in the annealed iPP films may show volume dilatation during necking, being in disagreement with the constant

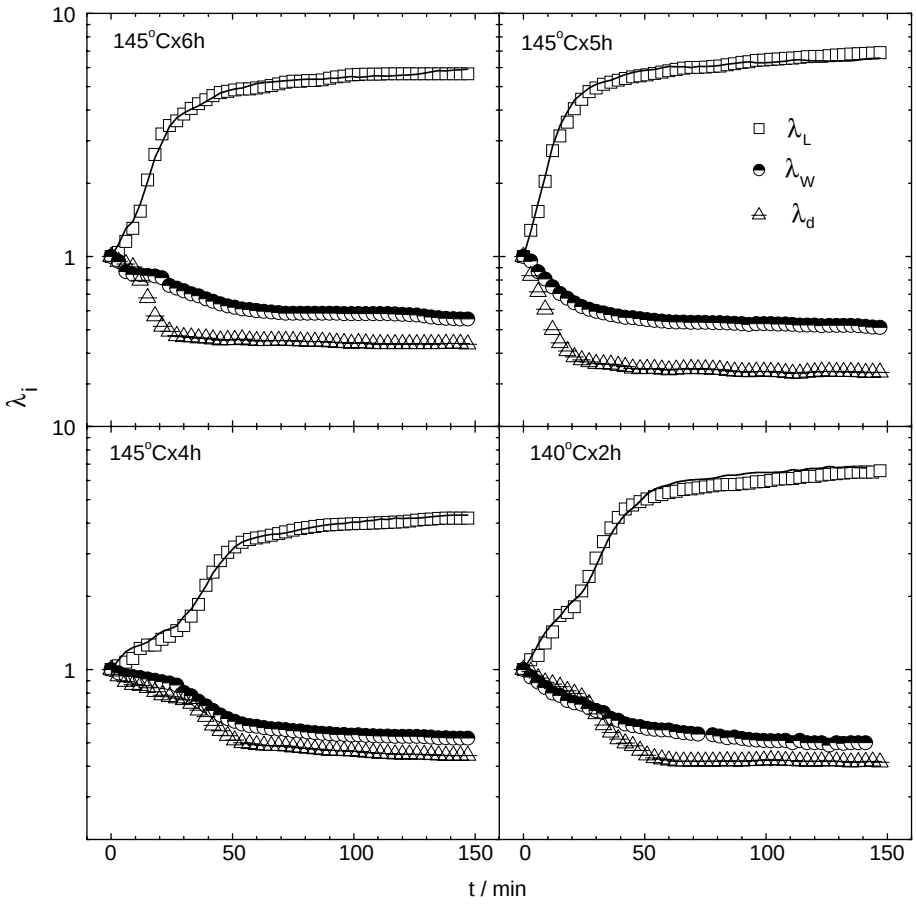


Fig. 4. Local draw ratios $\lambda_L$, $\lambda_W$ and $\lambda_d$ from the predetermined sampling area as a function of the stretching time $t$. The solid curves show $\lambda_L$ calculated from $\lambda_W$ and $\lambda_d$ by assuming an identical value of Poisson's ratio $\nu$ in the deformation.

volume deformation of the quenched sample. The samples 145 °C×6 h and 140 °C×2 h show $\nu$ very close to each other while the sample 145 °C×4 h undergoes constant volume deformation being the same as the quenched sample. Therefore, the volume dilatation is not directly related to the preparation condition but rather to the morphological characteristic of the samples.

The microcrystalline region in the annealed samples may contain submicron spherulites or spherulitic embryos on the submicron scale, which could not be distinguished under polarized optical microscope. Deformation just beyond the yield point introduces microcavities between spherulites or between lamellae perpendicular to draw direction [19]. As a characteristic of plastic local instability in uniaxial tension, microcavitation process might facilitate the transition from the lamellar to the fibrillar morphology during the plastic deformation. Sakaoku and Peterlin [20] found that microfibrils with lateral dimensions of ~20 nm originate in micronecks at crack boundaries of the original crystal lamellae and exhibit maximum local strain separated by large regions of much less deformed material. With increasing draw ratio, the inhomogeneity of strain in adjacent bundles of microfibrils creates a great many longitudinal microvoids with more or less disoriented microfibrils bridging the gaps. The microcavities appear before any large scale breakup of the crystals and their formation is a necessary precursor [21] to intralamellar shear when amorphous chains are constrained in the cross-hatched lamellae or crystal shear is difficult because of the cross-hatching crystalline habit in the annealed iPP films. As microcavities are initiated, they grow along the draw direction and result in the volume dilatation shown in Fig. 4. When the microcavitation is absent as in sample 145 °C×4 h, the plasticity in lamellae may develops mainly according to crystallographic mechanisms [22]. After the sampling area is located in the neck entity, the slow increases in $\lambda_W$ and $f_{av}$ in Figs. 4 and 2(b), respectively, suggest that the microcavitation might occur simultaneously with the molecular deformation.

### 3.4. Application of the interpenetrating network model

Fig. 5(a) and (b), respectively, shows plots of $f_{av}$ and true stress $\sigma$ against $\lambda_L$ in the predetermined sampling area. The sample 145 °C×4 h undergoing a constant volume deformation endures the highest stress and the molecular orientation is the largest at the same level of $\lambda_L$ in comparison with the other three samples showing volume dilatation. The two samples 145 °C×6 h and 140 °C×2 h with $\nu = 0.40$ and 0.41, respectively, give rise to the lowest stress very close to each other up to $\lambda_L = 4$. However, molecules in these two samples are oriented to different degrees at the same level of $\lambda_L$. It

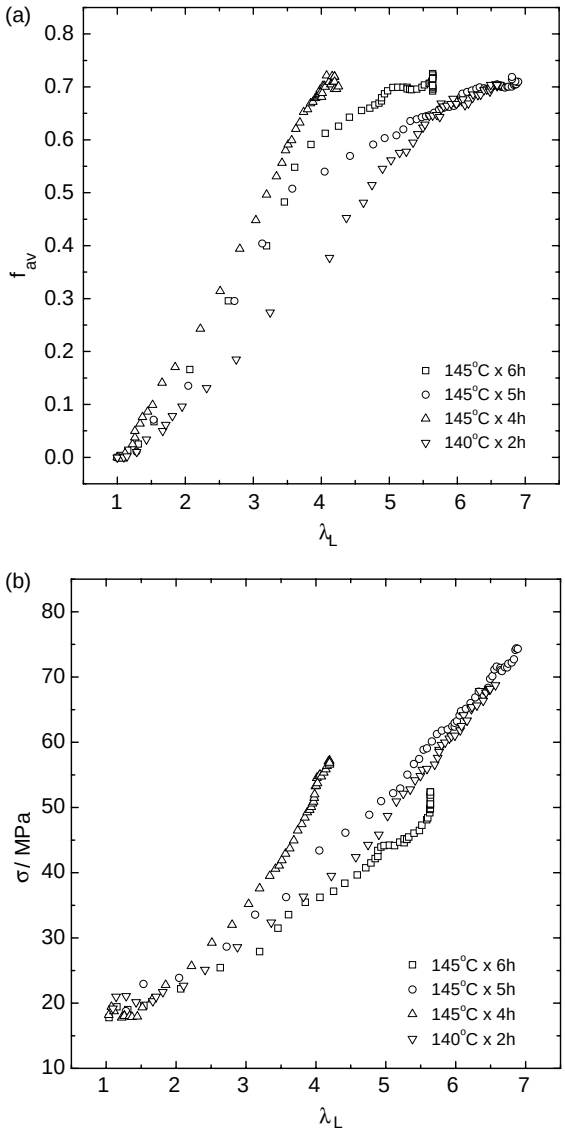


Fig. 5. Average orientation function $f_{av}$ (a) and true stress $\sigma$ (b) as a function of local draw ratios $\lambda_L$.

seems that the volume dilatation might be directly related to the deformational stress. The result in Fig. 5(b) reveals that the deformational stress after yielding increases with decreasing annealing time when the films were annealed at 145 °C. However, $f_{av}$ in Fig. 5(a) does not show a consistent tendency for these three samples, suggesting that annealing time does not affect the orientation behavior in the same manner as the local deformation. In fact, both the annealing condition (temperature and time) and the volume dilatation contribute to the molecular orientation and structure development in the microcrystalline region during stretching at room temperature.

It is distinct that microcavitation facilitates crystallites to undergo a relaxation owing to a change in the local stress field around the cavity. The release of concentrated local stress prevents most of the crystallites from breakdown, resulting in the capability to develop large strain before macroscopic breakage. Occurrence of microcavitation leads the observed strain to be undoubtedly larger than the actual strain of deformed macromolecules. For discussion of the other plastic deformation modes, it is better to remove the influence of microcavitation.

Here, it is worth mentioning the pioneering work of Ward [23] for studying the molecular orientation and mechanical behavior of polymer fibers in terms of a network deformation model. The mechanical properties and structures could be related to the network draw ratio determined by matching true stress–strain curves for the drawn and the initial fibers [24]. Recently, Penning et al. [25] found that true stress–strain tensile curves of melt spun nylon-6 and nylon-4,6 yarns from different origin can be shifted along the strain axis to form a master curve, representative of the degree of orientation during the previous processing steps. Using this method, Shirataki et al. [26] constructed true stress–strain master curve for poly(ethylene terephthalate) fibers with wide ranges of molecular orientation and crystallinity. They found that the fibers appear to behave in the manner of an almost ideal rubber

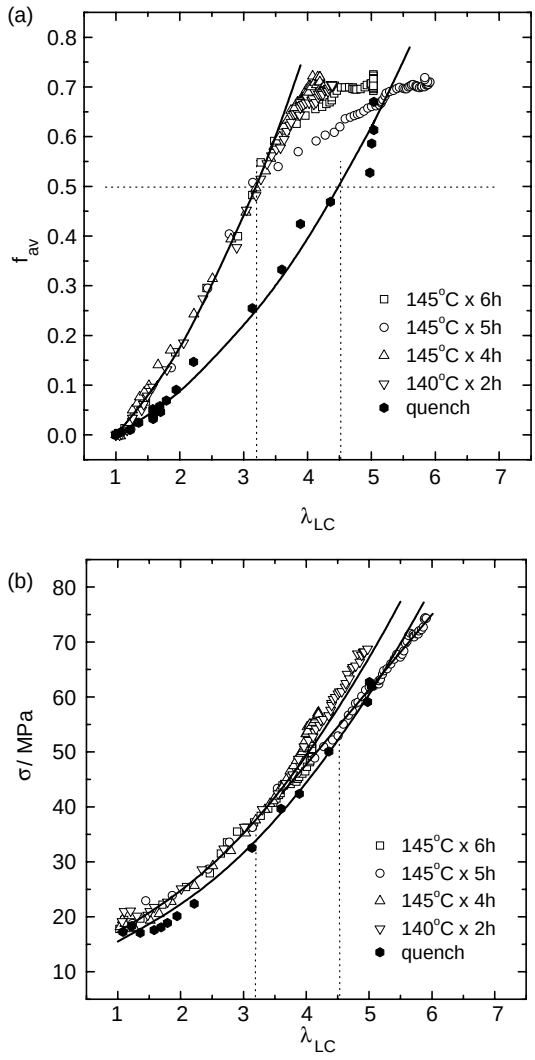


Fig. 6. Average orientation function $f_{av}$ (a) and true stress $\sigma$ (b) as a function of the corrected local draw ratios $\lambda_{Lc}$. The solid curves in (a) and (b) are fitted according to Eqs. (1) and (2), respectively.

during cold drawing and the initial molecular orientation and crystallinity do not affect the intrinsic network structure significantly.

Construction of master curves to $f_{av}$ and $\sigma$ against $\lambda_L$ seems helpful for discussing the molecular orientation and the mesoscale deformation behaviors of iPP films in absence of microcavitation. In this study, the master curves could be conveniently obtained by making correction of $\lambda_L$ to the samples 145 °C×6 h, 145 °C×5 h, and 140 °C×2 h so that their $f_{av}$ and $\sigma$ can be respectively overlapped onto those of the sample 145 °C×4 h. By introduction of a factor $a$ with $a=1$ when $\nu=0.5$, we correct the local strain $\lambda_L-1$ to $\lambda_{Lc}-1=(\lambda_L-1)a$ and $f_{av}$ and $\sigma$ are plotted against $\lambda_{Lc}$ in Fig. 6(a) and (b), respectively. Though the relation between $a$ and $\nu$ is ambiguous, it is seen that such attempt to obtain the master curves for the four samples is apparently successful at $\lambda_{Lc}<3.2$. The success of the superposition suggests that, under the condition of constant volume deformation, the underlying mechanism besides the volume dilatation in the samples 145 °C×6 h, 145 °C×5 h, and 140 °C×2 h is same as the sample 145 °C×4 h at $\lambda_{Lc}<3.2$ or $f_{am}<0.5$.

According to the result from the quenched sample, the amorphous phase behaves elastically at room temperatures above its glass transition temperature. Because that the molecular orientation of α-crystallites in the annealed films is closely related to the deformation of the surrounding amorphous chains whenever most of the crystallites keep their mechanical integrity (Fig. 3), $f_{av}$ as a function of $\lambda_{Lc}$ should give a molecular description of the deformation during the necking. The data in Fig. 6(a) should thus be fitted to the affine deformation model with an adjustable parameter $C$ [27]

$$f_{av}=C(\lambda_{Lc}^2-\lambda_{Lc}^{-1}) \tag{1}$$

The solid curve with $C=0.050$ well describes the $\lambda_L$ dependence of $f_{av}$ up to $f_{av}\approx0.50$, suggesting that the films deform pseudo-affinely on a mesoscale despite of the volume dilatation. Because the amorphous chains and crystallites are oriented toward the draw direction simultaneously with the occurrence of microcavitation, the pseudo-affine deformation is reasonable only when the molecular relaxation does not exceed the orientation. $f_{av}\approx0.50$ might correspond to the previous value of $f_{am}\approx0.45$ for the fully extended amorphous chains in the quenched film [9]. We have shown in the quenched film that $f_c$ as a function of $f_{am}$ deviates from the linear relationship due to the dominative plastic deformations in the crystalline phase after the amorphous chains are fully stretched [8]. This should also hold true in the annealed films, which causes the measured $f_{av}$ values to become lower than the prediction of Eq. (1).

The aforementioned results reveal the pseudo-affine deformation mode on a mesoscale for the microcrystalline region in the four annealed films. It may thereby be worthwhile to examine applicability of the interpenetrating network model [9] to the true stress–strain behaviors. This model simply assumes that the total true stress $\sigma$ after yielding is given as the sum of the true stresses, $\sigma_C$ and $\sigma_{CEAM}$, supported by the C and the CEAM networks, respectively, as

$$\sigma=\sigma_C+\sigma_{CEAM} \tag{2a}$$

$$\sigma_C=\sigma_y(C) \tag{2b}$$

$$\sigma_{CEAM}=M_{PT}(\lambda_{Lc}^2-\lambda_{Lc}^{-1}) \tag{2c}$$

Here $\sigma_y(C)$ is the true yield stress of the C network and $M_{PT}$ is the apparent shear modulus of the CEAM network, which are treated as adjust parameters for data fitting of the measured true stress–strain data in Fig. 6(b). It is shown that Eq. (2) with $\sigma_y(C)=17.2$ MPa and $M_{PT}=2$ MPa fairly describes the true stress–strain relationship in the strain range where Eq. (1) is applicable. At high strains, $\sigma$ becomes smaller than the model prediction for the samples 145 °C× 6 h and 145 °C×5 h, whereas, the reverse is observed for the other two samples.

The data are compared with those (solid symbol μ in Fig. 6) from the quenched sample with $\nu=0.5$ [8]. $f_{av}$ as a function of $\lambda_{Lc}$ in the annealed samples increases much faster than that in the quenched sample with $C=0.025$. The difference in parameter $C$ is related to the Kuhn segment number in the amorphous phase and the local crystallinity in the sampling area. The master curve of $\sigma$ against $\lambda_{Lc}$ of the annealed samples is located at the upper position of the true stress–strain curve of the quenched sample with $\sigma_y(C)=$ 15.5 MPa and $M_{PT}=1.8$ MPa. Annealing introduces cross-hatched α-crystallites in the microcrystalline region and a consequent increases in the lamellar thickness and the crystallinity, which causes $\sigma_y(C)$ to be higher than that in the quenched one. In other words, the C-network becomes somewhat rigid due to annealing. The higher $M_{PT}$ value in the annealed samples is related to a higher crystallinity in comparison with the quenched sample.

At high strains when the sampling area is located in the highly necked down region, $f_{av}$ as a function of $\lambda_{Lc}$ (Fig. 6(a)) clearly discloses a molecular orientation fashion differing from the pseudo-affine mode in the neck shoulder. Indeed, in the highly necked region after the amorphous chains are fully stretched, deformational stress is effectively concentrated on the crystallites, which leads to plastic deformations involving in chain slippage [28], lamellar fragmentation, stress-induced crystallization and decrystallization [29], fibrillation [30] or alteration of crystal structure. Nevertheless, without structure analysis (for example, X-ray diffraction) data sensitive to the crystalline phase in the predetermined sampling area, $f_{av}$ against $\lambda_{Lc}$ itself could not distinguish which microstructural mode is significant for deformation in the neck entity. An alternative way is to make an evaluation on the basis of deviation of the overlapped true stress–strain data from the prediction of the interpenetrating network model. The upward derivation occurred in the samples 145 °C×4 h and 140 °C× 2 h is mainly induced by the strain-induced crystallization and/or fibrillation incorporating the parallel orientated lamellar blocks and the strain-induced crystalline segments [31], while

the downward derivation in the samples 145 °C×6 h and 145 °C×5 h is due to destruction of crystallites and/or strain-induced alteration of crystal type. For $\lambda_{Lc}>3.5$, $\sigma$ increases almost linearly with $\lambda_{Lc}$ for the samples 145 °C×6 h and 145 °C×5 h and reaches the stress level of the quenched sample from $\lambda_{Lc}=4.5$, implying that the existing α-crystallites in these two samples are quite defective and most of them are transformed into the less ordered smectic form by the mechanical disruption [32] in the range of $3.5<\lambda_{Lc}<4.5$. With further increase in local strain, the deformation is rather in good agreement with that of the quenched sample. Therefore, the annealing time has a marked effect on the plastic deformation of the crystalline phase at the late stage of deformation in the microcrystalline region.

## 4. Conclusion

The local deformation in the microcrystalline region of four annealed iPP films is studied executing simultaneous measurements of MicIR dichroism, mesoscale strain, and macroscopic stress during unixial stretching at a constant elongation rate and at room temperature. Volume dilatation might be an important characteristic in the deformation of the annealed films except for the sample 145 °C×4 h. The true stress–strain and the $f_{av}$–$\lambda_L$ curves of the annealed samples showing volume dilatation can be overlapped onto those of the sample undergoing constant volume deformation, which can be conveniently achieved by corrected the local strain $\lambda_L-1$ to $\lambda_{Lc}-1=(\lambda_L-1)a$ using a reduction factor $a$. The $\sigma$–$\lambda_{Lc}$ relationship can be formulated using the interpenetrating network model up to $\lambda_{Lc}<3.2$, where the pseudo-affine deformation is also validated in the $f_{av}$–$\lambda_{Lc}$ relationship. The annealing condition has an important influence on the molecular orientation and deformation behavior. The neck propagates rather smoothly in the samples 145 °C×6 h and 145 °C×5 h while the neck shoulder might change its shape along with the necking propagation in the samples 145 °C×4 h and 140 °C×2 h. The deformation at high local strains after amorphous chains are fully stretched involves two kinds of plastic microstructural transformations in the crystalline phase, which causes $f_{av}$ and $\sigma$ to deviate from the model predictions. In the samples 145 °C×4 h and 140 °C×2 h, the strain-induced crystallization and fibrillation leads to the upward derivation of $\sigma$ from the model prediction in the overlapped plot. On the other hand, dominative plastic mechanism is the α-to-smectic crystal transformation at $3.5<\lambda_{Lc}<4.5$ in the samples 145 °C×6 h and 145 °C×5 h, which can be considered as one of annealing time effects.

## Acknowledgements

This work has been partially supported by the Grant-in-Aid for the Scientific Research from Ministry of Education, Culture, Sports, Science and Technology, Japan (No. 10305070) and one of the authors, Y. Song, is grateful to JSPS for the Grant-in-Aid for JSPS Fellows relating to JSPS Fellowship for Foreign Researchers (No. 12000317) during his stay in Japan for a postdoctoral research.

## References

[1] Lin L, Argon A. J Mater Sci 1994;29:294.
[2] Zhou H, Wilkes GL. J Mater Sci 1998;33:287.
[3] (a) Drozdov AD, Christiansen JdeC. Int J Solids Struct 2003;40:1337.
(b) Drozdov AD, Christiansen JdeC. Polymer 2003;44:1211.
(c) Drozdov AD, Gupta RK. Int J Eng Sci 2003;41:2335.
[4] Coulon G, Castelein G, G'Sell C. Polymer 1999;40:95.
[5] (a) Hiss R, Hobeika S, Lynn C, Strobl G. Macromolecules 1999;32:4390.
(b) Hobeika S, Men Y, Strobl G. Macromolecules 2000;33:1827.
(c) Men Y, Strobl G. J Macromol Sci, Phys B 2001;40:775.
(d) Men Y, Strobl G. Chin J Polym Sci 2002;20:161.
[6] Shigematsu Y, Takada A, Nemoto N, Nitta K. Rev Sci Instrum 2001;72:3927.
[7] Song Y, Shigematsu Y, Nitta K-H, Nemoto N. Polym J 2002;34:584.
[8] Song Y, Nitta K-H, Nemoto N. Macromolecules 2003;36:1955.
[9] Song Y, Nitta K-H, Nemoto N. Macromolecules 2003;36:8066.
[10] Vadimsky RG, Keith HD, Padden FJ. J Polym Sci 1969;7:1367.
[11] Takayanagi M, Nitta K-H. Macromol Theory Simul 1997;6:181.
[12] Song Y, Nemoto N. Polymer 2005;46:6522.
[13] Song Y, Yamamoto H, Nemoto N. Macromolecules 2004;37:6219.
[14] Naka Y, Nemoto N, Song Y. J Polym Sci, Part B: Polym Phys. Polym Phys 2005;43:1520.
[15] (a) Karger-Kocsis J, Varga J, Ehrenstein GW. J Appl Polym Sci 1997;64:2057.
(b) Tjong SC, Shen JS, Li RKY. Polym Eng Sci 1996;36:100.
[16] Song Y, Nitta K-H, Nemoto N. J Soc Rheol Jpn 2003;31:131.
[17] Snyder RG, Schachtschneider JH. Spectrochim Acta 1964;20:853.
[18] (a) Siesler HW. Adv Polym Sci 1984;65:1.
(b) Samuels R. J Makromol Chem Suppl 1981;4:241.
[19] Castagnet S, Gacougnolle JL, Dang P. Mater Sci Eng A 2000;276:152.
[20] Sakaoku K, Peterlin A. J Polym Sci, Part A-2: Polym Phys 1971;9:895.
[21] Bowden PB, Young RJ. J Mater Sci 1974;9:2034.
[22] Oleinik EF. Polym Sci Ser C 2003;45:17.
[23] Ward IM. J Macromol Sci.-Phys B 1967;1:667.
[24] Long SD, Ward IM. J Appl Polym Sci 1991;42:1911.
[25] (a) Penning JP, Van Ruiten J, Brouwer R, Gabriëlse W. Polymer 2003;44:5869.
(b) Ruiten J, Riedel R, Deblieck R, Brouwer R, Penning JP. J Mater Sci 2001;36:3119.
[26] Shirataki H, Nakashima A, Sato K, Okajima K. J Appl Polym Sci 1997;64:2631.
[27] (a) Kuhn W, Grun F. Kolloid Z 1942;101:248.
(b) Nagai K. J Chem Phys 1964;40:2818.
(c) Reo RJ, Krigbaum J. J Appl Phys 1964;35:2215.
[28] Clausst B, Salem DR. Macromolecules 1995;28:8328.
[29] Peterlin A. J Mater Sci 1971;6:490.
[30] Kestenbach H-J, Petermann J. Polymer 1994;35:5217.
[31] Peterlin A. Colloid Polym Sci 1975;253:809.
[32] (a) Somani RH, Hsiao BS, Nogales A, Srinivas S, Tsou AH, Sics I, et al. Macromolecules 2000;33:9385.
(b) Corradini P, Petraccone V, De Rosa C, Guerra G. Macromolecules 1986;19:2699.
(c) Corradini P, De Rosa C, Guerra G, Petraccone V. Polym Commun 1989;30:281.